
Princeton Plasma Physics Laboratory

PPPL-

PPPL-



Prepared for the U.S. Department of Energy under Contract DE-AC02-09CH11466.

Princeton Plasma Physics Laboratory

Report Disclaimers

Full Legal Disclaimer

This report was prepared as an account of work sponsored by an agency of the United States Government. Neither the United States Government nor any agency thereof, nor any of their employees, nor any of their contractors, subcontractors or their employees, makes any warranty, express or implied, or assumes any legal liability or responsibility for the accuracy, completeness, or any third party's use or the results of such use of any information, apparatus, product, or process disclosed, or represents that its use would not infringe privately owned rights. Reference herein to any specific commercial product, process, or service by trade name, trademark, manufacturer, or otherwise, does not necessarily constitute or imply its endorsement, recommendation, or favoring by the United States Government or any agency thereof or its contractors or subcontractors. The views and opinions of authors expressed herein do not necessarily state or reflect those of the United States Government or any agency thereof.

Trademark Disclaimer

Reference herein to any specific commercial product, process, or service by trade name, trademark, manufacturer, or otherwise, does not necessarily constitute or imply its endorsement, recommendation, or favoring by the United States Government or any agency thereof or its contractors or subcontractors.

PPPL Report Availability

Princeton Plasma Physics Laboratory:

<http://www.pppl.gov/techreports.cfm>

Office of Scientific and Technical Information (OSTI):

<http://www.osti.gov/bridge>

Related Links:

[U.S. Department of Energy](#)

[Office of Scientific and Technical Information](#)

[Fusion Links](#)

Effects of magnetic field on the turbulent wake of a cylinder in MHD channel flow

John R. Rhoads¹,
Eric M. Edlund² and Hantao Ji²

¹Department of Astrophysical Sciences, Princeton University, Princeton, NJ 08544, USA

²Princeton Plasma Physics Laboratory, Princeton, NJ 08543, USA

(Received 12 April 2013)

Results from a free-surface MHD flow experiment are presented detailing the modification of vortices in the wake of a circular cylinder with its axis parallel to the applied magnetic field. Experiments were performed with a Reynolds number near $Re \sim 10^4$ as the interaction parameter, $N = |\mathbf{j} \times \mathbf{B}|/|\rho(\mathbf{v} \cdot \nabla)\mathbf{v}|$, was increased through unity. By concurrently sampling the downstream fluid velocity at sixteen cross-stream locations in the wake, it was possible to extract an ensemble of azimuthal velocity profiles as a function of radius for vortices shed by the cylinder at varying strengths of magnetic field. Results indicate a significant change in vortex radius and rotation as N is increased. The lack of deviations from the vortex velocity profile at high magnetic fields suggests the absence of small-scale turbulent features. By sampling the wake at three locations downstream in subsequent experiments, the decay of the vortices was examined and the effective viscosity was found to decrease as $N^{-0.49 \pm 0.04}$. This reduction in effective viscosity is due to the modification of the small-scale eddies by the magnetic field. The slope of the energy spectrum was observed to change from a $k^{-1.8}$ power-law at low N to a $k^{-3.5}$ power-law for $N > 1$. Together, these results suggest the flow smoothly transitioned to a quasi-two-dimensional state in the range $0 < N < 1$.

1. Introduction

Studying the flow past a cylinder is a classical experiment used to investigate the transition to turbulence. However, in electrically conducting fluids turbulent structures can change dramatically in the presence of a magnetic field due to their ability to support internal currents. Experiments described in this paper investigate the transition that occurs in the wake of an obstruction as an applied magnetic field is increased while holding the fluid velocity constant.

The experiments presented in this paper considered flows with a Reynolds number $Re = v_\infty L/\nu > 9000$ where v_∞ is the free-stream fluid velocity, L is the cylinder diameter and ν is the kinematic viscosity. This value of Re falls into what is commonly referred to as the shear-layer transition regime for hydrodynamic flows (Williamson 1996, pp. 489,520-524). In this regime, the wake retains many of the features present in a Von Kármán street, which evolves at lower Reynolds numbers ($Re = 50 - 200$) before the transition to turbulence. However, in the shear-layer transition regime the discrete alternating vortices of the Von Kármán street become localized regions of vorticity, with small-scale three-dimensional turbulent features superimposed on larger vortex structures with a size on the order of the obstruction diameter (Wei & Smith 1986; Williamson *et al.* 1995). Excellent visualizations of both laminar and turbulent Von Kármán streets are included by Van Dyke (1982, p. 31,56-57). As a matter of convention, the larger regions

Reynolds number	$Re \equiv \frac{ \rho(\mathbf{v} \cdot \nabla) \mathbf{v} }{ \mu \nabla^2 \mathbf{v} }$ $= \frac{v_\infty L}{\nu}$	Ratio of inertial to viscous terms
Interaction parameter	$N \equiv \frac{ \mathbf{j} \times \mathbf{B} }{ \rho(\mathbf{v} \cdot \nabla) \mathbf{v} }$ $= \frac{\sigma L B_0^2}{\rho v_0}$	Ratio of electromagnetic to inertial terms
Hartmann number	$Ha^2 \equiv \frac{ \mathbf{j} \times \mathbf{B} }{ \mu \nabla^2 \mathbf{v} }$ $= h^2 B_0^2 \left(\frac{\sigma}{\mu} \right)$	Ratio of electromagnetic to viscous terms

TABLE 1. Dimensionless parameters.

of circulation will be referred to as ‘vortices’ in this paper, which may in turn contain smaller-scale ‘eddies’ due to the turbulent nature of the flow.

While small-scale, three-dimensional eddies are expected for a hydrodynamic flow in this turbulent regime, the addition of a magnetic field imposes a constraint on the fluid motion through Ohmic dissipation. In particular, eddies with vorticity misaligned with the applied magnetic field, \mathbf{B} , experience a torque exerted by the field while eddies initially aligned with \mathbf{B} elongate along the magnetic field lines (Davidson 1997, 2001, pp. 122-132). By restricting fluid motion, the field causes the flow to become quasi-two-dimensional (see Alemany *et al.* 1979), thereby affecting the energy cascade as proposed by Kolmogorov and others for hydrodynamic systems (Kolmogorov 1941; Kraichnan 1967; Frisch 1995). The transition from three- to two-dimensional behavior of the flow was observed to be a smooth function of the strength of the applied field in the experiments described herein.

Ever since the work of Strouhal (1878), the flow separation of the fluid as it moves past an object has been studied extensively over a wide range of both geometries and Reynolds numbers in the laboratory (see Williamson 1996). Most work has focused on hydrodynamic behavior, although some work was done on the effect of an applied magnetic field on an electrically conductive fluid. Several experimental groups investigating MHD flows made point measurements in the wake behind a cylinder in various geometries to study the fluctuation levels in addition to the shedding mechanism and shape of the wake (Kolesnikov & Tsinober 1972; Papailiou & Lykoudis 1974; Lahjomri *et al.* 1993; Branover *et al.* 2004). Experiments were also conducted with a duct-flow experiment using an array of probes at the wall to estimate the vorticity of structures in the wake of a cylinder (Frank *et al.* 2001). However, earlier results did not include detailed measurements of the internal velocity structure of the vortices. The results presented in this paper complement the previous work by providing a look into the internal velocity profile of vortices and allowing inferences to be made regarding MHD turbulence.

Kolesnikov, Sommeria and Moreau among others posited that the introduction of the magnetic field creates a quasi-two-dimensional system through ohmic dissipation as described above. Several groups experimentally and/or theoretically investigated this phenomenon by artificially driving turbulent-like states (Kolesnikov & Tsinober 1974; Sommeria & Moreau 1982; Sommeria 1986; Zikanov & Thess 1998; Alboussière *et al.* 1999;

Thess & Zikanov 2007; Klein *et al.* 2009). Sreenivasan & Alboussière (2002) in particular studied the decay of an artificially created vortex subjected to an axial magnetic field and found that for $N \gg 1$, the MHD forces arising from induced currents within the flow dominate the damping of the vortex and render viscous dissipation almost entirely negligible. However, Sreenivasan did not report detailed measurements for $N \leq 1$, which is the regime most closely examined in this work. Many of these previous experiments observed a change in the spectral slope and/or reported to have seen evidence of the so-called ‘inverse cascade’.

Several groups have also worked on computational modeling of the wake behind a bluff body in MHD flow. In particular, Mück *et al.* (2000, p. 279) performed 3D MHD simulations that showed the collimation of shed vortices at a moderate Reynolds number of 250, indicating a clear transition to a two-dimensional state somewhere in the range $0.2 \leq N \lesssim 1$, qualitatively agreeing with experimental observations by Branover *et al.* (2004, p. 294) showing the wake undergoing a transition in the range $0.5 < N < 1$. Dousset & Pothérat (2008) presented results from a finite volume code at high Hartmann number, and although the shedding frequency qualitatively agrees, the behavior of the shed vortices varies considerably from the results presented in this paper. Direct quantitative comparison of the internal velocity profiles of the vortices with computational results was not available.

2. Background

The introduction of an external magnetic field requires an additional term in the Navier-Stokes equations. For closure, Ohm’s law, Faraday’s law, and Ampere’s law must also be included along with the typical incompressibility condition. That is

$$\rho \left(\frac{\partial \mathbf{v}}{\partial t} + (\mathbf{v} \cdot \nabla) \mathbf{v} \right) = -\nabla p + \mu \nabla^2 \mathbf{v} + \mathbf{j} \times \mathbf{B}, \quad (2.1)$$

$$\mathbf{j}/\sigma = \mathbf{E} + \mathbf{v} \times \mathbf{B}, \quad (2.2)$$

$$\nabla \times \mathbf{E} = 0, \quad (2.3)$$

$$\nabla \times \mathbf{B} = \mu_0 \mathbf{j}, \quad (2.4)$$

$$\nabla \cdot \mathbf{v} = 0, \quad (2.5)$$

where ρ is the fluid density, \mathbf{v} is the velocity, p is the pressure, μ is the dynamic viscosity, \mathbf{j} is the current density, \mathbf{B} is the magnetic field, σ is the conductivity of the fluid, \mathbf{E} is the electric field, and μ_0 is the magnetic permeability of the fluid. The effects of the induced magnetic field are negligible when $R_m = \mu_0 \sigma v_\infty h \ll 1$, where h is the fluid depth. For experiments presented in this paper, $R_m < 10^{-2}$. In this ‘inductionless limit’, electric fields can be expressed as purely electrostatic as seen in 2.3 and a scalar potential ($\mathbf{E} = -\nabla\phi$) can be introduced. The displacement current has also been neglected in Ampere’s law, equation 2.4, giving rise to a solenoidal current density ($\nabla \cdot \mathbf{j} = 0$).

As the applied magnetic field increases, the electromagnetic contribution to the Navier-Stokes equations becomes more significant to the dynamics of the flow. The ratio of the contribution of the electromagnetic term to the inertial term in equation 2.1 is often referred to as the interaction parameter (also called the Stuart number), N . Similarly, the ratio of electromagnetic to viscous forces is defined as the square of the Hartmann number, Ha , as shown in table 1. In this work, the characteristic length, L , is defined as the cylinder diameter, v_0 is defined as the mean fluid velocity in the wake, v_∞ is defined as

the free-stream fluid velocity and B_0 is defined as the magnitude of the applied magnetic field. For Ha and R_m , h is taken to be the fluid depth due to the geometry of the experiment.

Practically, because the flow velocity is held constant for each set of experiments (to within 5%), N scales like B_0^2 while Ha scales like B_0 . For $N \gtrsim 0.5$ some of the effects of the magnetic field are experimentally observed to saturate, in agreement with results from other experiments in various geometries mentioned previously (see Harris 1960; Lahjomri *et al.* 1993; Mück *et al.* 2000; Branover *et al.* 2004).

In order to quantify changes to the wake of the cylinder as N was increased, the vortex velocity profiles measured in the wake were fit to a Rankine vortex velocity profile. This vortex model consists of a core with constant angular velocity surrounded by a free vortex. As will be shown shortly, the abrupt transition between these two regions gives rise to viscous dissipation. The velocity profile for a Rankine vortex is given by $v_r = v_z = 0$ and

$$v_\phi(r) = \begin{cases} \Gamma r / (2\pi R^2), & r \leq R \\ \Gamma / (2\pi r), & r > R, \end{cases} \quad (2.6)$$

where $\Gamma = \oint v_\phi ds = 2\pi\omega R^2$ is the circulation of a vortex of radius R and angular velocity ω . For this purely azimuthal flow, the velocity of a stationary vortex will evolve according to

$$\begin{aligned} \frac{\partial \mathbf{v}}{\partial t} &= \nu \nabla^2 \mathbf{v}, \\ \frac{\partial v_\phi}{\partial t} &= \nu \left(\frac{\partial^2 v_\phi}{\partial r^2} + \frac{1}{r} \frac{\partial v_\phi}{\partial r} - \frac{v_\phi}{r^2} \right). \end{aligned} \quad (2.7)$$

Analytically, the viscous damping can be seen easily by noting that each region of the Rankine vortex in equation 2.6 is a Taylor-Couette solution ($\mathbf{v}(r) = (c_1 r + c_2/r)\hat{\phi}$), which satisfies both $\nabla^2 \mathbf{v} = 0$ and $\nabla \cdot \mathbf{v} = 0$. However, the discontinuous derivative at $r = R$ of the Rankine profile will result in a non-zero value of the Laplacian at the transition, resulting in local damping. As the vortex viscously damps, the profile will deviate from the constituent Taylor-Couette solutions, and will thereby undergo further damping away from the peak as seen in figure 6(a). Heuristically, the time-scale for this dissipation can be derived

$$\frac{\partial \mathbf{v}}{\partial t} = \nu \nabla^2 \mathbf{v} \sim \frac{4\nu}{R^2} \mathbf{v},$$

using the half-width of the radius of the eddy as a typical length scale for velocity gradients. This relation implies that viscous forces will gradually smooth out the profile on the timescale of $\tau \approx R^2/4\nu$ for a laminar vortex (Aboelkassem *et al.* 2005). However, eddies within a turbulent vortex will interact more strongly than a laminar sheared flow and will ultimately smooth the velocity profile faster, decreasing τ and increasing the effective viscosity, ν_{eff} .

Sommeria & Moreau (1982) pointed out that at high Hartmann number, there is an additional term to account for Hartmann damping that should be included in equation 2.7. Namely,

$$\frac{\partial \mathbf{v}}{\partial t} = \nu \nabla^2 \mathbf{v} - \frac{2B}{R} \left(\frac{\sigma\nu}{\rho} \right)^{1/2} \mathbf{v}. \quad (2.8)$$

The effect of this additional term was observed in some results and will be addressed in more detail in section 4.3. As a caveat, equation 2.8 was derived for duct flow with two

Parameter	Symbol	Value
Density	ρ	6360 kg/m ³
Kinematic viscosity	$\nu = \mu/\rho$	2.98x10 ⁻⁷ m ² /s
Conductivity	σ	3.1x10 ⁶ S/m

TABLE 2. Physical properties of Ga⁶⁷In^{20.5}Sn^{12.5} alloy (Morley *et al.* 2008).

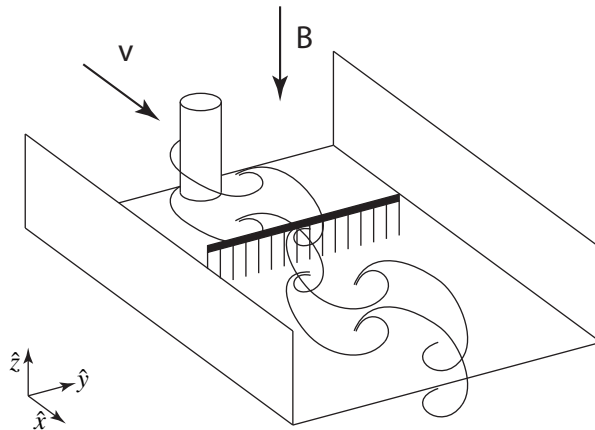


FIGURE 1. Experimental setup showing vertical field aligned with cylinder axis and the velocity probe array.

distinct Hartmann layers. Due to the free surface in this experiment, the Hartmann layer at the surface of the fluid is slightly different, which may affect the direct applicability of this additional damping term to these experiments.

3. Experimental Setup

The experiments described in this paper were conducted in a acrylic channel 80 cm in length by 16 cm in width positioned horizontally in a uniform, vertical magnetic field perpendicular to the free surface of the fluid. A static cylinder 19 mm in diameter was placed in the flow with its axis aligned with the magnetic field as illustrated in figure 1. The cylinder diameter corresponded to a blockage ratio of about 12% and vortex interaction with the walls of the channel was minimal. The working fluid was a gallium-indium-tin eutectic described in table 2 that flowed through the channel with a depth of about 1 cm at speeds around 15 cm/s.

An array of sixteen potential probes was inserted into the wake of the cylinder from the free surface to make measurements of the downstream fluid velocity. The potential probes operate by measuring the local EMF created from the motion of the conductive fluid through the magnetic field. The measured value of the local potential represents the average velocity over the distance between the probe tips, also called the probe width. The spatial resolution of the probes was limited to about 4.5 mm compared to the 19

mm cylinder diameter. Structures within the flow smaller than the probe width cannot be resolved directly.

The operating principle of the potential probes can be derived from Ohm's law (eq. 2.2). By inserting the probes into the core of the flow, $\mathbf{j} \approx 0$, yielding $-\mathbf{E} \approx \mathbf{v} \times \mathbf{B}$. Using this approximation and replacing \mathbf{E} with $-\nabla\phi$ from the electrostatic assumption, one obtains $\nabla\phi = \mathbf{v} \times \mathbf{B}$. Integrating over the distance between probe tips (chosen to lie in the proper orthogonal direction) the potential is found to be $\phi(v_x) = \bar{v}_x d B_z$ where $\bar{v}_x = \frac{1}{d} \int_0^d v_x(y) dy$. Others (see Sommeria 1986; Kljugin & Thess 1998; Sreenivasan & Alboussière 2002) have discussed the error arising from internal currents on the measured potential. Experimentally, the probe signals were found to be indicative of the fluid velocity for values of $Ha > 5$. The spatial averaging effect due to the finite probe width was taken into account when fitting the velocity profiles, although this artifact was negligible in most cases.

In theory, the probe separation could be reduced in order to increase the spatial resolution; however, this is technically difficult for two reasons. First, the measured potentials are linear in probe width. By reducing the probe width, the signal is reduced by the same factor, resulting in a higher signal-to-noise ratio and reducing the quality of the measurements. Secondly, each of the probe tips has a finite thickness required for both structural integrity and in order to ensure good electrical contact with the fluid. By decreasing the probe separation, more probes would need to be inserted into the flow to characterize the wake. The additional probes would be more likely to disrupt the bulk flow and compromise the measurements.

Sequential experiments were conducted with the cylinder located roughly three, five and fourteen diameters upstream from the potential probe array. For each cylinder location, the magnetic field was scanned from a value of 150 gauss to 2500 gauss, corresponding to a range of $0.01 \leq N \leq 8$ based on cylinder diameter and free-stream velocity or $5 \leq Ha \leq 100$ as calculated based on the fluid depth. Time series from each of the probes after amplification were recorded and the data logged via PC. For each set of experiments at a fixed cylinder location, the volumetric flow rate was held constant as the magnetic field was scanned. However, a 25% variation in the flow rate between experimental sets at different cylinder positions was observed during the analysis. This variation in free-stream velocity was due to the lack of a reliable global flow rate measurement at the time, but was deemed inconsequential in regard to the fluctuations because the flow is well within the shear-layer transition regime. The variation in flow rate is only directly relevant to certain quantities identified in the following section. For a given cylinder position, the fluid velocity varied no more than 5% as the magnetic field was scanned.

4. Results

The calibrated potential probes indicated flow velocities of 10.6, 13.5 and 11.6 cm/s in the wake of the cylinder and free-stream velocities of 14.0, 17.8 and 13.9 cm/s for experiments at three, five and fourteen diameters respectively. However, this variation in the free-stream velocity and the systematic uncertainty in the absolute calibration of the probe array does not affect the fluctuation amplitude nor the spectra of the probe signals. Only the rotation rate, circulation and N are affected by the absolute calibration of the probes. Where applicable, the uncertainties in calculated quantities have been propagated throughout the analysis.

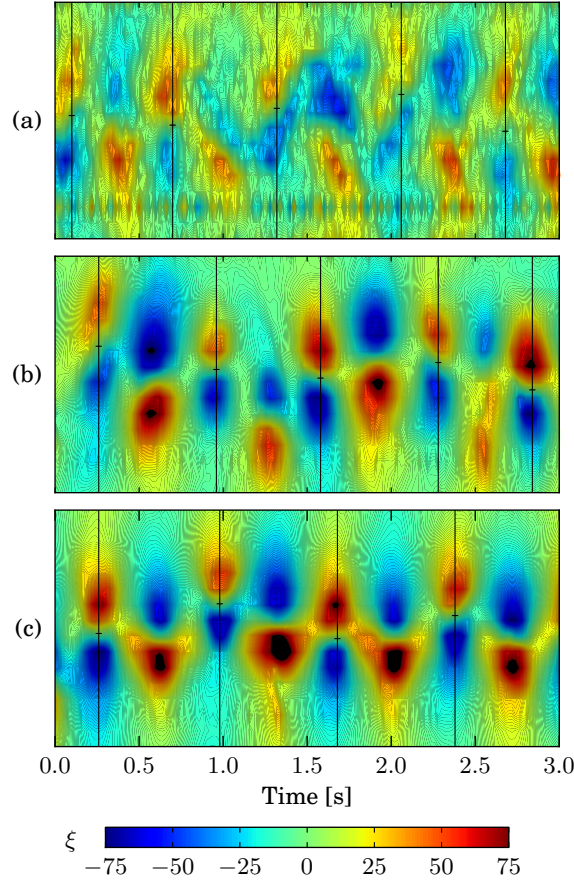


FIGURE 2. Contours of velocity fluctuations in the wake approximately three diameters behind cylinder as a function of cross-channel position and time at (a) $N = 0.01$, (b) $N = 0.66$ and (c) $N = 1.85$.

4.1. Identifying Vortices

In order to eliminate slight variations in absolute calibration from one probe to another and to remove the background flow, the potential probes were self-normalized to provide the most self-consistent picture of the downstream velocity fluctuations across the channel. The background flow is approximated as the time-average, $\langle v_x(y) \rangle$, and the fluctuation amplitude was defined as

$$\xi(y, t) = \frac{v_x(y, t) - \langle v_x(y) \rangle}{\langle v_x(y) \rangle} \cdot 100.$$

By plotting ξ as a function of cross-stream position and time, the wake of the cylinder can be visualized as seen in figure 2. Over the entire range of interaction parameter values, a clear Von Kármán street was observed. Each pair of lobes represents a vortex passing the fixed probe array in time.

Since the velocity probes only measure the stream-wise component of the velocity, $\xi(y, t)$ will only represent the azimuthal velocity of a vortex when the center of the vortex is aligned with the probe array as it is convected downstream. Additionally, the center of the vortex in the cross-stream direction must also be located in order to define

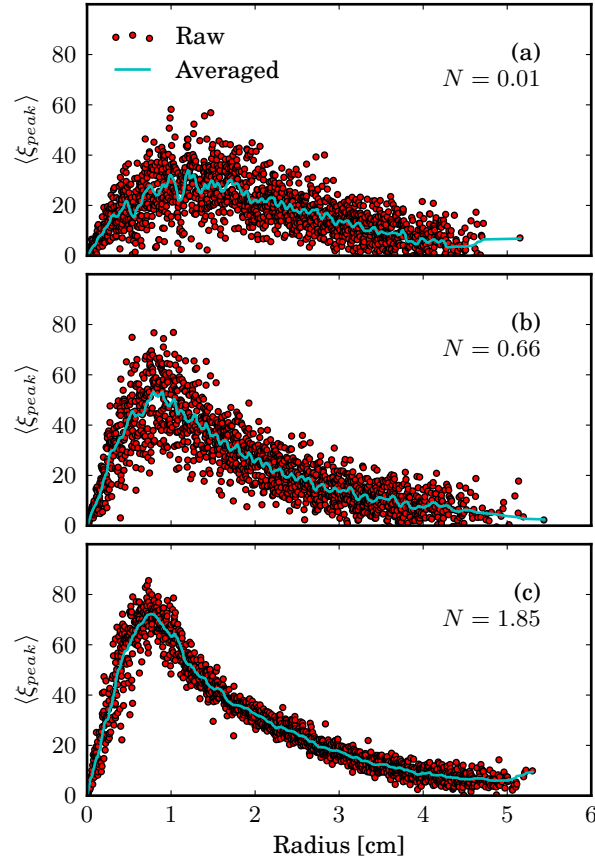


FIGURE 3. Radial velocity profile of vortices at (a) low and (b) moderate and (c) high interaction parameter, three diameters into wake. Profiles correspond to contours in Figure 2

$r = 0$. Therefore, each vortex must be found in two dimensions: x (down-stream) and y (cross-stream).

In order to locate the center of the vortex in the x direction, local maxima in time of the $\text{RMS} = (\int |\xi(y, t)|^2 dy)^{1/2}$ of the measured velocity profile were found. This point in time coincides with the point when the vortex is centered underneath the probes and ξ exactly matches the azimuthal component of the vortex velocity. The maxima in time are indicated in figure 2 by vertical lines. Once the vortex probe-crossing time was found, the zero-crossing point of the ξ -profile was identified with a linear interpolation. This point indicated the location of the vortex in the y direction and is shown in figure 2 by horizontal dashes. The coordinates of the velocity profile were then shifted such that $r = 0$ corresponds to the point where $v = 0$ using a linear interpolation. If any vortices did not meet the criteria for selection, that is if the local maximum of the RMS was ambiguous or the center of the vortex fell near the edge of the probe array, the vortex was neglected and excluded from the aggregate profile.

The key advance to the approach outlined above is using the random location of the shed vortices (in the cross-stream direction) to produce a statistical collection of indicative profiles, effectively providing a high spatial resolution measurement of the vortex velocity profile. That is, as the streamlines reconnect and each vortex separates

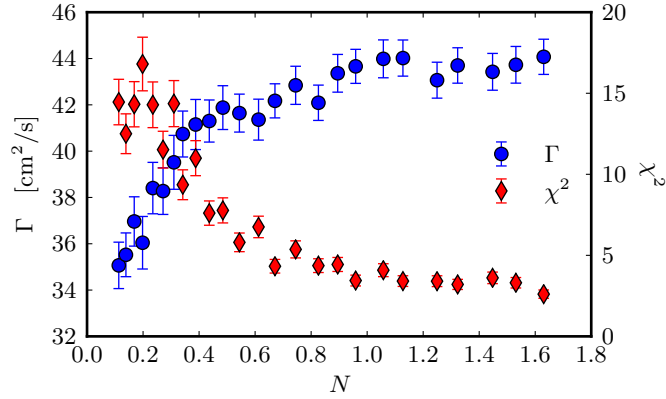


FIGURE 4. Total circulation and chi-squared of measured profile from the average profile versus interaction parameter five diameters into wake.

from the cylinder, the center of the shed vortex is slightly displaced a distance δ from the centerline of the channel. Moreover, at high Reynolds number as the vortices are convected downstream and the wake spreads, δ fluctuates relative to the probe positions. Therefore, as the shed vortex flows past the fixed array of velocity probes, the probe array is able to sample the internal velocity profile of each vortex at a slightly different location. The result can be seen in figure 3, which shows the conglomerate velocity profiles corresponding to the vertical lines seen in figure 2.

4.2. Vortex Characteristics

By implementing the technique described in section 4.1, an ensemble of velocity profiles was collected. The average of the ensemble was assumed to be representative of the average vortex for a given field strength and can be seen in figure 3.

For clarity, the velocity profile shown in figure 3 is the upstream component of vortices with positive vorticity, even though the entire vortex profile was sampled and used in the analysis. The complete velocity profile was approximately symmetric about the center of the vortex. However, it was observed that the downstream component of the vortex (the side of the vortex supplementing the fluid velocity) had a slightly different velocity profile than the upstream component. This effect will not be discussed in the current paper. The profiles corresponding to vortices of positive and negative vorticity showed no discernible difference for a given vortex street (other than their sign) and were therefore combined when discussing trends in radius, rotation and circulation.

The measured azimuthal velocity profile at low fields varies considerably as seen in figure 3(a) and (b), likely due to the presence of small-scale turbulent eddies and the effect of averaging over fine structures by the probes. However, by identifying at least 150 vortices of both positive and negative vorticity, a reasonable average can be calculated. At higher field strengths, it was observed that vortices become much more consistent and coherent, resulting in a very clear radial velocity profile with very little deviation as shown in figure 3(c).

The presence of small-scale turbulent eddies was investigated by examining the spread of the ensemble relative to the average velocity profile of the vortex. At low fields, the individual radial velocity profiles have significant deviations from the averaged profile, indicative of irregular, turbulent fluctuations on top of the global rotation. One metric for the coherency of the vortex and by extension the absence of eddies is the variance

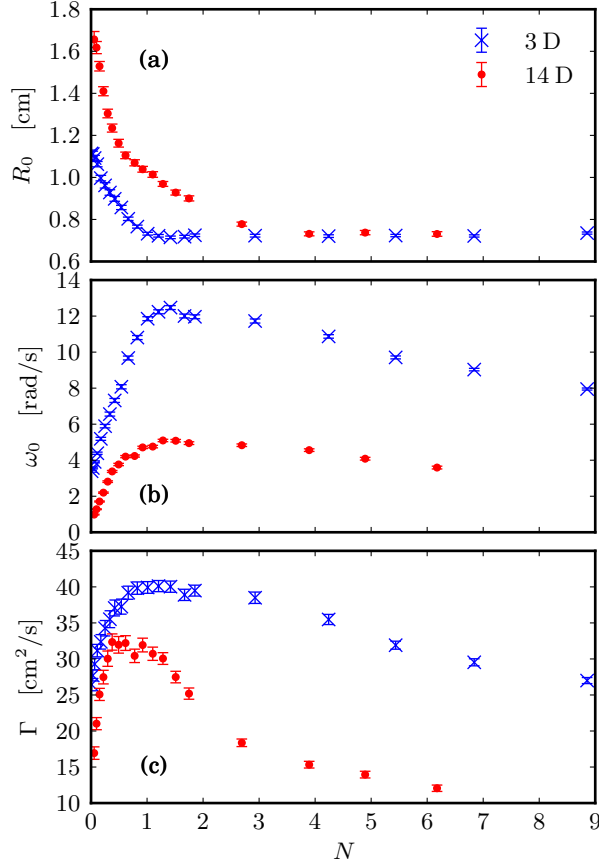


FIGURE 5. Trends of (a) radius, (b) rotation and (c) circulation of vortices versus interaction parameter at three and fourteen diameters into the wake.

or χ^2 of the ensemble over the smoothed profile. Once the flow has become quasi-two-dimensional, the fluctuations on top of the global rotation are dramatically reduced as seen in figure 4.

Figure 4 also shows the measured circulation as a function of interaction parameter. Excepting low N , the circulation of the vortices tends to remain constant until Hartmann damping alters the fluid motion at high N , to be discussed below. At low N , the measurement of the circulation is unreliable because of the limited spatial resolution of the velocimetry diagnostic explained as follows. The (hydrodynamic) Kolmogorov length scale for these flows is

$$\eta = \frac{L}{Re^{3/4}} \approx 25 \mu\text{m}.$$

Hence, many eddies much smaller than the spatial resolution of the potential probes will exist at low N as a consequence of the turbulent cascade. Recall that the circulation is essentially a metric for the total angular momentum of the vortex. Because of the limitation in spatial resolution of the diagnostic, there is no contribution to the measured angular momentum by eddies smaller than the probe width, resulting in a measured circulation artificially depressed at $N < 0.5$. Figure 4 shows that above $N \sim 0.5$, both the

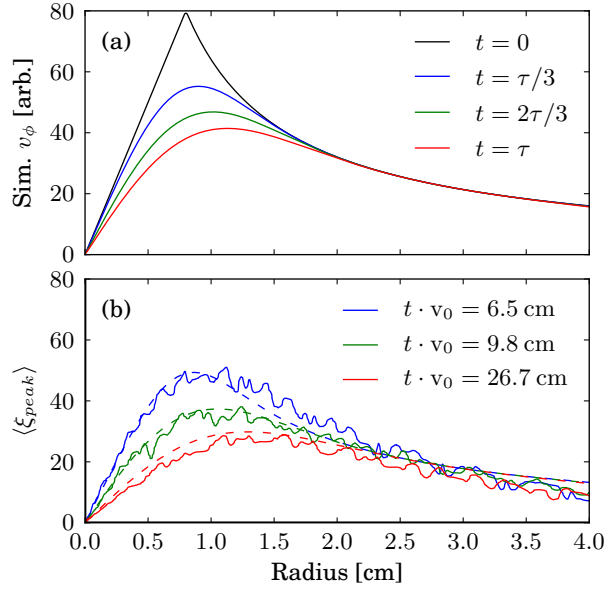


FIGURE 6. Viscous vortex damping seen in (a) simulation of Rankine profile, $\tau = R^2/4\nu$ and (b) radial velocity profiles at $N = 0.4$ (0.7 kG) at three positions downstream in the wake. Dashed lines represent the best fitting profiles from the simulations.

circulation and the calculated variance from the profiles plateau, indicating the absence of eddies smaller than the probe separation distance and signaling the transition to a quasi-2D state.

It was observed that at low magnetic fields, the rotation rate of the vortices increases linearly with the field, while the radius of the core decreases to about 7.5 mm. This can be observed in figures 5(a) and (b). As N increases above 2, Hartmann braking introduced in equation 2.8 begins to play a factor in damping the rotation of the vortices, explaining the roll-off of the rotation rate at the higher field strengths. This can be seen in figures 5(b) and (c) which shows the rotation rate and the the global angular momentum reduced via a torque exerted by the magnetic field.

4.3. Vortex Decay

For a fixed flow velocity and location in the wake, the measured profiles were observed to be far less damped for $N \sim 1$ than for $N < 1$. This is clearly illustrated in figures 3(a) and (c), where the vortex three diameters into the wake is much less damped at the higher magnetic field from the lack of turbulent dissipation. As mentioned previously, the change in damping is a result of the magnetic field restricting turbulent structures in the flow, thereby reducing the effective viscosity and subsequent damping of the velocity profile. Once the vortex profiles were collected at three positions in the wake of the cylinder, it was possible to artificially examine the spatiotemporal decay of the vortices as a function of the applied magnetic field. By looking only at normalized profiles, the results from each of the three cylinder locations can be compared over the range $0.01 < N < 2$.

The calibrated fluid velocity was used to infer the time from inception of the vortices until they passed the probe array. This approach made it possible to examine the evolution of the velocity profile for a each field strength as seen in figure 6(b). These sequential profiles were then used to calculate the effective viscosity. First, a relaxed Rankine profile

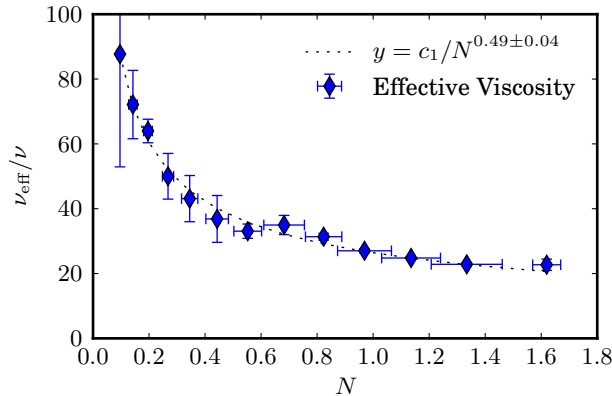


FIGURE 7. Effective viscosity as a function of interaction parameter.

was fit to the experimental profile at three diameters into the wake. The experimental profile was iteratively compared to simulated profiles evolving according to equation 2.7 with varying radii as a function of time as seen in figure 6(a). After identifying the best-fitting profile (in both radius and time) for the experimental measurements made three diameters into the wake, the experimental profiles from five and fourteen diameters downstream were then fit in a similar manner to the temporal decay of the same seed vortex of fixed radius and amplitude. From the ratio of the experimental time extracted from the location of the cylinder relative to the probes and fluid velocity of the wake to the simulated time corresponding to the best fit, the effective viscosity was calculated for the remaining two locations. Figure 7 shows the effective viscosity decreasing with $N^{-0.49 \pm 0.04}$ over a range corresponding to $0.1 \leq N \leq 1.7$, before Hartmann damping of the vortices became prevalent.

Despite its presence at $N > 2$, the electromagnetic damping term in equation 2.8 was neglected when comparing the decay of the experimental profiles for two reasons. First of all, the contribution from this term was experimentally observed to be small at $N \leq 2$ as seen in figure 4 which shows no appreciable decrease in the circulation over the range of interest. Secondly and perhaps more importantly, this linear damping term accounting for Hartmann braking merely scales the amplitude of the entire velocity profile and does not alter its shape. Only viscous damping broadens the velocity profile and accounts for the outward shift in the peak velocity observed in figure 6. Figure 6(b) shows that the experimental data undergoes a very clear outward shift in the maximum velocity as the amplitude decays. Adding a linear damping term to account for Hartmann braking would result in an unaccountable decrease in amplitude, resulting in poorly fitting profiles. For these reasons, only turbulent viscous damping described in equation 2.7 was considered when examining the decay of the vortices for an interaction parameter near unity.

The scaling of the effective viscosity agrees with the ‘Joule cone’ theoretical predictions by Sommeria & Moreau (1982, p. 514), which suggest that the permissible region of phase-space in the $k_{\perp} - k_{\parallel}$ plane scales as $N^{-1/2}$ for $N \gg 1$, where k_{\parallel} represents a variation in the direction of \mathbf{B} . Essentially, as N is increased, variations along \mathbf{B} are restricted by the magnetic field, causing the flow to become more quasi-two-dimensional. Although this theory was derived for $N \gg 1$, these results may suggest that the scaling persists at moderate N as well. This constraint on k_{\parallel} and reduction in three-dimensionality could perhaps explain the absence of small-scale structures as a consequence of the inverse cascade in two-dimensional flow.

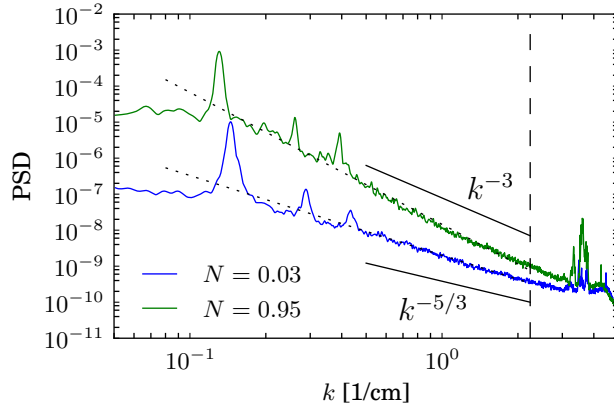


FIGURE 8. Power spectra of probe signal from three diameters into the wake at two values of N . Dotted lines indicate fit used to extract the power-law scaling. The vertical dashed line represents the spatial resolution limit of the probes.

4.4. Signs of two-dimensionalization

Conceptually, the two-dimensionalization of the flow could be characterized by a number of observables. The experiments in this paper exploit two particular features. First, by measuring velocity fluctuations in the fluid, the energy spectra can be approximated. For conventional hydrodynamic turbulence, this spectra is expected to follow a $k^{-5/3}$ power law, often called the Kolmogorov scaling of the energy cascade. Similar principles used to derive the five-thirds scaling can be applied to two-dimensional turbulence, giving rise to a k^{-3} scaling (neglecting logarithmic corrections). While subtle, this change in spectral slope can be observed by looking at the power spectral density of the velocity fluctuations. In this paper, Taylor's hypothesis is employed to relate ω and k in order to obtain the energy spectra as a function of wavenumber from time series of velocity fluctuations.

As can be seen in figure 8, the energy spectrum of the flow was observed to transition from a Kolmogorov-like hydrodynamic state with a near $k^{-5/3}$ power law to a $k^{-3.5}$ power law as N was increased. The vertical dashed line represents the spatial limitation of the probes. It can also be pointed out that the Strouhal number, a non-dimensional frequency defined as $St = fD/v_\infty$ where D is the cylinder diameter, f is the shedding frequency and v_∞ is the free-stream fluid velocity, was observed to remain relatively constant as the field strength was increased. The large peak of both curves near $k = 0.1$ in figure 8 represents the primary shedding frequency and illustrates the lack of dependence of the shedding mechanism on the magnetic field for these values of interaction parameter.

Moreover, the smooth transition of the spectral slope between a hydrodynamic power-law to a two-dimensional power-law was observed to occur over the range $0 < N < 1$ as seen in figure 9, agreeing with other evidence of the transition presented in this paper. Due to the finite magnetic field required for the operation of the velocity diagnostic, a pure 'hydrodynamic' measurement could not be made for comparison. However, figure 9 clearly indicates a trend towards $\gamma = 5/3$ as $N \rightarrow 0$.

The second characteristic employed to examine the two-dimensionality of the flow is the inverse-cascade and the corresponding enstrophy ($\Omega = \frac{1}{2}\langle|\boldsymbol{\omega}|^2\rangle$) cascade present in two-dimensional flows. It is shown by others (see Frisch 1995; Kraichnan 1967; Sommeria 1986) that structures at small scales in a two-dimensional system will transfer energy to the largest scale possible. This implies that small turbulent eddies will coalesce into large,

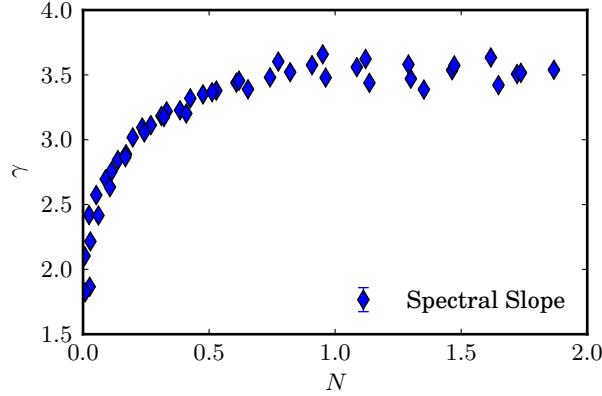


FIGURE 9. Spectral slope of power spectra versus N showing smooth transition from 3D to 2D turbulence.

coherent vortices, which could explain the trends in the spread of the measured velocity profiles and in the global angular momentum. Particularly, recall that the measured circulation increased at low N in figure 4. As explained in section 4.2, the diagnostic could not resolve the contribution of eddies smaller than the probe width to the global angular momentum. It can be argued that the majority of these eddies will have the same sign vorticity as the vortex due to the shedding mechanism as the fluid separates from the side of the obstruction. Making this assumption, if the eddies were to participate in an inverse cascade to measurable scales, their angular momentum would be conserved, resulting in an increase in the measured global angular momentum as observed in the experiments.

The two-dimensionalization of the flow not only affects the measured circulation, but also explains the trends observed in the radius and rotation rates of the vortices. It was observed that the vortices tend to decrease in size as the magnetic field is increased until the radius of the vortex matches the injection scale, as seen in figure 5(a). The observed decrease in radius for $N < 1$ could be a result of the merging of the constituent eddies, concentrating the circulation at the injection scale. In the hydrodynamic cases, the small-scale eddies act to rapidly diffuse the vortex's core of rotation, resulting in a larger region of circulation. If the eddies were to merge in an inverse cascade at $N \sim 1$, not only would the effective viscosity go down, but the angular momentum of the merging eddies would be conserved, resulting in the increased rotation rate as seen in figure 5(b).

5. Conclusion

The internal velocity profile of eddies shed from a vertical cylinder was presented as a function of the applied vertical magnetic field. A novel approach for isolating the radial velocity profiles of vortices in the wake of a cylinder was developed. From these velocity profiles, the effects of the magnetic field on turbulent structures within the flow were inferred.

The radii of vortices were observed to decrease with applied magnetic field, likely due to a reduction in the effective viscosity as a result of the magnetic field altering small-scale eddies. Meanwhile, the rotation rate of the vortices for values of interaction parameter in the range of $0 \leq N < 2$ was observed to increase so as to conserve total angular momentum (or global circulation, Γ) within the capabilities of the diagnostic resolution.

At $N > 2$, Hartmann braking damped the motion of the vortices, resulting in a reduction in Γ .

The prevalence of small-scale turbulent features has been shown to decrease significantly as N approaches ~ 0.5 . Above this threshold, the magnetic field alters the evolution of the eddies as evidenced by both the decrease in the χ^2 of the measured velocity profiles and in the significant reduction in effective viscosity.

Results suggest the possibility of an inverse cascade as a consequence of the flow becoming quasi-two-dimensional. Measurements of the velocity fluctuations in the wake of a cylinder at moderate Re indicate the characteristic change in spectral slope associated with two-dimensional turbulence. The transition in the spectral slope was observed to occur as N approaches ~ 0.5 , coinciding with the transition observed with other metrics. Further, the apparent lack of small-scale features in magnetized cases along with the conservation of angular momentum suggests a mechanism through which small eddies coalesce, a la an inverse cascade.

By examining the decay of the vortices, it was found that the effective viscosity scales like $N^{-0.49 \pm 0.04}$. The effect of the magnetic field on small-scale eddies, namely the coalescence mentioned above along with the ‘Joule cone’ restriction on $k_{||}$, is thought to be the most probable explanation for the significant reduction in effective viscosity.

It is evident that the imposed magnetic field introduces a preferred direction for the vorticity of vortices within the fluid, which results in macroscopic behavior significantly different than that without a magnetic field.

The authors would like to acknowledge the contributions of Peter Sloboda, Erik Spence and several undergraduate interns to this work. Additionally, the authors would like to thank André Thess for his useful discussion and suggestions during the preparation of the manuscript. This work was supported under US DOE contract DE-AC02-09CH11466.

REFERENCES

- ABOELKASSEM, Y., VATISTAS, G.H. & ESMail, N. 2005 Viscous dissipation of Rankine vortex profile in zero meridional flow. *Acta Mech Sinica* **21**, 550–556.
- ALBOUSSIÈRE, T., USPENSKI, V. & MOREAU, R. 1999 Quasi-2D MHD turbulent shear layers. *Exp. Thermal and Fluid Science* **20**, 19–24.
- ALEMANY, A., MOREAU, R., SULEM, P.L. & FRISCH, U. 1979 Influence of an external magnetic field on homogeneous MHD turbulence. *Journal de Mécanique* **18** (2), 277–313.
- BRANOVER, H., EIDELMAN, A., GOLBRAIKH, E., KAPUSTA, A. & MIKHAILOVICH, B. 2004 Wave–mean flow interaction in an MHD wake behind bluff body. *Fluid Dynamics Research* **35**, 287–298.
- DAVIDSON, P.A. 1997 The role of angular momentum in the magnetic damping of turbulence. *J. Fluid Mech.* **336**, 123–150.
- DAVIDSON, P.A. 2001 *An Introduction to Magnetohydrodynamics*. Cambridge, UK: Cambridge University Press.
- DOUSSET, V. & POTHÉRAT, A. 2008 Numerical simulations of a cylinder wake under a strong axial magnetic field. *Phys. Fluids* **20**, 017104.
- FRANK, M., BARLEON, L. & MÜLLER, U. 2001 Visual analysis of two-dimensional magnetohydrodynamics. *Phys. Fluids* **13** (8), 2287–2295.
- FRISCH, U. 1995 *Turbulence*. Cambridge, UK: Cambridge University Press.
- HARRIS, L.P. 1960 *Hydromagnetic channel flows*. Technology Press.
- KLEIN, R., POTHÉRAT, A. & ALFERENOK, A. 2009 Experiment on a confined electrically driven vortex pair. *Phys. Rev. E* **79**, 016304.
- KLJUKIN, A. & THESS, A. 1998 Direct measurement of the stream-function in a quasi-two-dimensional liquid metal flow. *Exp. in Fluids* **25**, 298–304.
- KOLESNIKOV, Y.B. & TSINOBER, A.B. 1972 Two-dimensional turbulent flow behind a circular

- cylinder. *Magnetohydrodynamics* **8**, 300–307, translated from *Magnitnaya Gidrodinamika* **3**, 23–31 (1972).
- KOLESNIKOV, Y.B. & TSINOBER, A.B. 1974 Experimental investigation of two-dimensional turbulence behind a grid. *Fluid Mechanics* **4**, 621–624, translated from *Isv. Akad. Nauk. SSSR Mekhanika Zhidkosti i Gaza* **4**, 146–150 (1974).
- KOLMOGOROV, A.N. 1941 The local structure of turbulence in incompressible viscous fluid for very large Reynolds' numbers. *Dokl. Akad. Nauk SSSR* **30** (4), 299–303, reprinted in *Proc. R. Soc. Lond. A* **434**, 9–13 (1991).
- KRAICHNAN, R. 1967 Inertial ranges in two-dimensional turbulence. *Phys. Fluids* **10** (7), 1417–1423.
- LAHJOMRI, J., CAPÉLAN, PH. & ALEMANY, A. 1993 The cylinder wake in a magnetic field aligned with the velocity. *J. Fluid Mech.* **253**, 421–448.
- MORLEY, N.B., BURRIS, J., CADWALLADER, L.C. & NORBERG, M.D. 2008 GaInSn usage in the research laboratory. *Rev. of Sci. Instr.* **79** (5), 056107.
- MÜCK, B., GÜNTHER, C., MÜLLER, U. & BÜHLER, L. 2000 Three-dimensional MHD flows in rectangular ducts with internal obstacles. *J. Fluid Mech.* **418**, 265–295.
- PAPAILIOU, D. & LYKOUDIS, P. 1974 Turbulent vortex streets and the entrainment mechanism of the turbulent wake. *J. Fluid Mech.* **62**, 11–31.
- SOMMERIA, J. 1986 Experimental study of the two-dimensional inverse energy cascade in a square box. *J. Fluid Mech.* **170**, 139–168.
- SOMMERIA, J. & MOREAU, R. 1982 Why, how, and when, MHD turbulence becomes two-dimensional. *J. Fluid Mech.* **118**, 507–518.
- SREENIVASAN, B. & ALBOUSSIÈRE, T. 2002 Experimental study of a vortex in a magnetic field. *J. Fluid Mech.* **464**, 287–309.
- STROUHAL, V. 1878 Ueber eine besondere Art der Tonerregung. *Ann. Phys. und Chem.* **15** (10), 216–251.
- THESS, A. & ZIKANOV, O. 2007 Transition from two-dimensional to three-dimensional magnetohydrodynamic turbulence. *J. Fluid Mech.* **579**, 383–412.
- VAN DYKE, M. 1982 *An Album of Fluid Motion*. Stanford, CA: Parabolic Press.
- WEI, T. & SMITH, C.R. 1986 Secondary vortices in the wake of circular cylinders. *J. Fluid Mech.* **169**, 513–533.
- WILLIAMSON, C.H.K. 1996 Vortex dynamics in the cylinder wake. *Ann. Rev. Fluid Mech.* **28**, 477–539.
- WILLIAMSON, C.H.K., WU, J. & SHERIDAN, J. 1995 Scaling of streamwise vortices in wakes. *Phys. Fluids* **7** (10), 2307–2309.
- ZIKANOV, O. & THESS, A. 1998 Direct numerical simulation of forced MHD turbulence at low magnetic Reynolds number. *J. Fluid Mech.* **358**, 299–333.

The Princeton Plasma Physics Laboratory is operated
by Princeton University under contract
with the U.S. Department of Energy.

Information Services
Princeton Plasma Physics Laboratory
P.O. Box 451
Princeton, NJ 08543

Phone: 609-243-2245
Fax: 609-243-2751
e-mail: pppl_info@pppl.gov
Internet Address: <http://www.pppl.gov>